10. P. K. Jackson, S. Chevalier, M. Philippe, M. W. Kirschner, *J. Cell Biol.* **130**, 755 (1995).
11. J. Y. Su, R. E. Rempel, E. Erikson, J. L. Maller, *Proc. Natl. Acad. Sci. U.S.A.* **92**, 10187 (1995).
12. J. J. Blow, *J. Cell Biol.* **122**, 993 (1993).
13. N. Mathias *et al.*, *Mol. Cell. Biol.* **16**, 6634 (1996); C. Bai *et al.*, *Cell* **86**, 263 (1996).
14. N. Satoh, *Dev. Growth Differ.* **19**, 111 (1977); J. Newport and M. Kirschner, *Cell* **30**, 675 (1982).
15. A. W. Murray and M. W. Kirschner, *Nature* **339**, 275 (1989); A. W. Murray, M. J. Solomon, M. W. Kirschner, *ibid.*, p. 280.
16. A. W. Murray, *Methods Cell Biol.* **36**, 581 (1991).
17. LSS was generated as described (*16*). Extracts replicated 75 to 100% of the input template (5 ng/μl). Cycloheximide (0.1 mg/ml) was added to LSS before replication was assayed.
18. Demembranated sperm nuclei were prepared as described (*4*) and used at a final DNA concentration of 5 ng/μl. Plasmid template ssM13 DNA was added to a 10 ng/μl final concentration. DNA replication was measured by trichloroacetic acid precipitation of radiolabeled fragments (*4, 10*) and presented as a percent replication of the input template (5 ng/μl). Alternatively, samples were ethanol precipitated, run on agarose gels, and autoradiographed.
19. Antibodies were covalently cross-linked to protein A (pA)–Sepharose (Seph) or pA-affiprep beads as described [E. Harlow and D. Lane, *Antibodies: A Laboratory Manual* (Cold Spring Harbor Laboratory, Cold Spring Harbor, NY, 1988)]. Immunodepletion was performed by mixing 1 volume LSS to 1.2 volumes antibody-coupled pA-Seph beads for 2 hours at 0°C with resuspension every 10 min.
20. LSS, Superdex column fraction, or eluted affiprep material were analyzed by SDS-PAGE, transferred to nitrocellulose, incubated with affinity-purified anti-hCDC34 immunoglobulin (Ig), and analyzed by enhanced chemiluminescence (Amersham).
21. Replication foci were analyzed by stated methods (*10, 12*).
22. Five volumes of LSS were incubated with one volume of coupled pA-affiprep beads for 3 hours at 4°C. Beads were washed with 15 volumes each of XB– [extract buffer: 100 mM KCl, 0.1 mM $CaCl_2$, 1 mM $MgCl_2$, and 10 mM Hepes (pH 7.7)] (one time), XB– with 500 mM KCl (three times), and 0.5× XB– (two times) (*23*). Immunodepleted LSS was added to the beads and assayed for replication. Alternatively, the washed beads were treated with 100 mM glycine (pH 2.5), and the eluate was neutralized with 1 M tris (pH 8). Samples were concentrated and analyzed by SDS-PAGE and silver stained or analyzed by immunoblotting.
23. S100 was generated by dilution of LSS with nine volumes 20 mM tris (pH 7.7), 100 mM KCl, 1 mM $MgCl_2$, and 1 mM dithiothreitol followed by centrifugation for 1 hour at 100,000*g*. S100 was concentrated to its original volume and loaded onto a HiLoad 16/60 Superdex 200 column (Pharmacia). Fractions were concentrated to one-tenth their volume and incubated with anti-hCDC34 affiprep beads for 2.5 hours at 0°C with resuspension every 10 min. Beads were washed with XB– supplemented with KCl to 500 mM (XB– with 500 mM KCl), added to Cdc34p-depleted LSS with sperm nuclei (5 ng/μl), and incubated at 23°C for 3 to 4 hours.
24. U. P. Strausfeld *et al.*, *Curr. Biol.* **4**, 876 (1994).
25. In vitro Xic1 degradation reaction was performed by adding sperm nuclei to a concentration of 7.9 ng/μl in 5 μl LSS, with 0.3 μl ivt Xic1, 0.25 μl energy regeneration (ER) mix (*16*), 1.25 mg/ml ubiquitin, 0.1 mg/ml cycloheximide, and incubation at 23°C. Reactions were stopped by adding 2× SDS-PAGE sample buffer. Xic1 was in vitro transcribed from the SP6 promoter of Xic1/pCS2+ [D. L. Turner and H. Weintraub, *Genes Dev.* **8**, 1434 (1994)] (subcloned from Xic1/pBluescript) and translated with [^{35}S]methionine. Xic1 bands were quantitated by phosphorimager (Molecular Dynamics), and Xic1 levels were normalized to the percent Xic1 remaining to determine half-life values.
26. Xic1 degradation was assayed as before (*25*) except 0.14 μl ivt [^{35}S]met-labeled Xic1 was used, and sperm nuclei were added to a concentration of 3.2 ng/μl (1000 nuclei/μl), 7.9 ng/μl (2500 nuclei/μl), or 15.8 ng/μl (5000 nuclei/μl) and incubated for 3 hours at 23°C.
27. We thank S. Plon for hCDC34/pGEX; J. Maller for baculovirus Cdk2–cyclin E, Cdk2, kinase-inactive Cdk2, and Xic1/pBluescript; A. Philpott for sperm nuclei and HSS; R. King for Δ90; V. Chau for sharing results before publication; J. Ruderman, D. Finley, A. Philpott, T. Boyer, R. King, P. Adams, and R. Davis for critical reading of the manuscript; A. Philpott, J. Peters, T. Boyer, R. King, and P. Jackson for helpful discussions; and the National Institutes of General Medical Science for support of this work. P.R.Y. is a fellow of the Jane Coffin Childs Memorial Fund.

24 January 1997; accepted 8 July 1997

X-ray Structure of Bacteriorhodopsin at 2.5 Angstroms from Microcrystals Grown in Lipidic Cubic Phases

Eva Pebay-Peyroula, Gabriele Rummel, Jurg P. Rosenbusch, Ehud M. Landau

Lipidic cubic phases provide a continuous three-dimensional bilayer matrix that facilitates nucleation and growth of bacteriorhodopsin microcrystals. The crystals diffract x-rays isotropically to 2.0 angstroms. The structure of this light-driven proton pump was solved at a resolution of 2.5 angstroms by molecular replacement, using previous results from electron crystallographic studies as a model. The earlier structure was generally confirmed, but several differences were found, including loop conformations and side chain residues. Eight water molecules are now identified experimentally in the proton pathway. These findings reveal the constituents of the proton translocation pathway in the ground state.

Bacteriorhodopsin (bR) is a light-driven proton-translocating pump that converts the energy of photons into an electrochemical potential (*1*). In the plasma membrane of *Halobacterium salinarium* (previously known as *H. halobium*), this integral membrane protein, which is located within the bilayer boundary, is tightly packed in two-dimensional crystals termed purple patches (*2*). The pioneering studies of Henderson and co-workers, who investigated unstained membranes by electron microscopy (EM) and image reconstruction (*3*) and by x-ray analyses (*4*), provided the first insight into the structural organization of a membrane protein at an intermediate resolution of 7 Å. Over the past 20 years, major advances in electron crystallography resulted in considerable improvements in resolution (*5*), which currently reaches 3.5 Å in the plane of the membrane and 4.3 Å perpendicular to it (*6*). These studies revealed that the structure of bR consists of seven membrane-spanning α helices that are connected by three external and three cytoplasmic loops (*7*). The pigment, retinal, is bound covalently (through a protonated Schiff base) to Lys^{216}. It is buried in the interior of the protein and is stabilized by the binding of the β-ionone ring in a hydrophobic pocket.

The function of bR has been studied extensively by a variety of structural, genetic, and spectroscopic methods and by molecular dynamics calculations (*6, 8–10*). The primary event, absorption of a photon, causes isomerization of the retinal from the all-trans to the 13-cis configuration. A series of intermediate events follows, including deprotonation of the Schiff base and proton transfer to Asp^{85}. Another proton is subsequently released, the Schiff base is reprotonated from Asp^{96}, and a proton is taken up from the cytoplasmic side. Thermal reisomerization of the retinal to the ground state completes the photocycle.

A detailed understanding of this mechanism requires knowledge of its structure at atomic resolution, an endeavor for which well-diffracting, highly ordered three-dimensional (3D) crystals appear most promising. Several attempts have been reported (*11*), but the crystals obtained were either too small or exhibited extensive mosaicity as a result of poor order along the *c* axis. To overcome these limitations, we devised a concept for the crystallization of membrane proteins by exploiting the properties of bicontinuous lipidic cubic phases (*12*). Membrane proteins, once inserted into this continuous, 3D curved lipid bilayer matrix, diffuse laterally to nucleate and eventually to yield well-ordered crystals. Our initial results with microcrystals of bR, which diffracted x-rays to 3.7 Å resolution (*12*), have

E. Pebay-Peyroula, Institut de Biologie Structurale/CEA-CNRS/Université Joseph Fourier, 41 Avenue des Martyrs, F-38027 Grenoble Cedex 1, France.
G. Rummel, J. P. Rosenbusch, E. M. Landau, Biozentrum, University of Basel, Klingelbergstrasse 70, CH-4056 Basel, Switzerland.

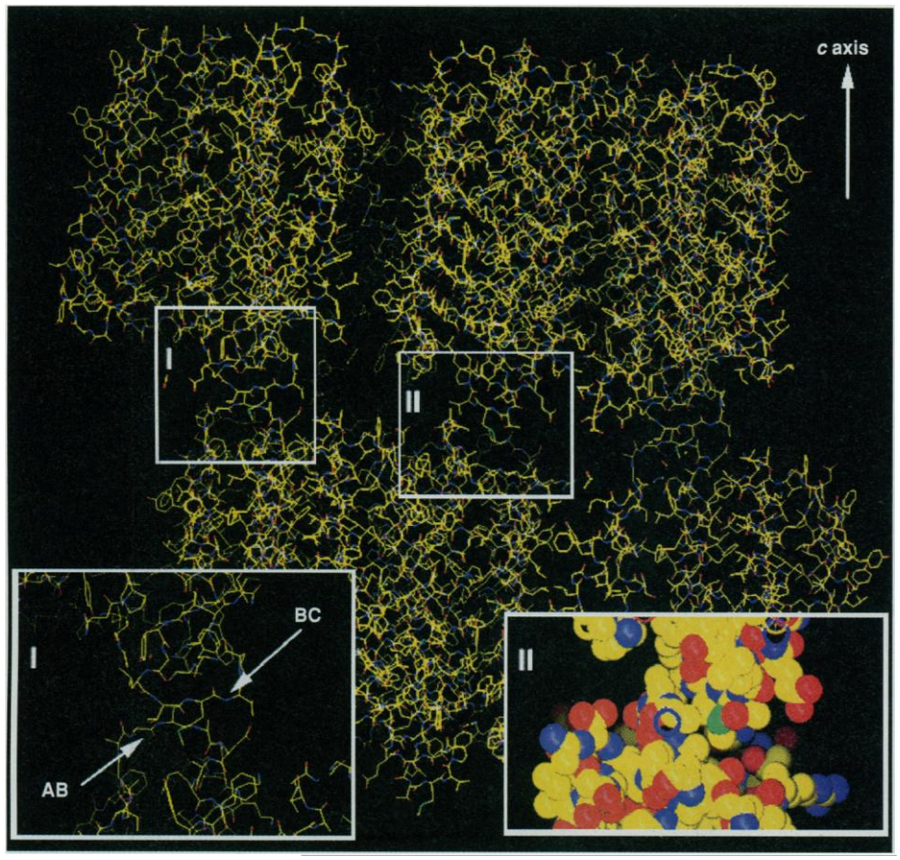

Fig. 1. Crystal packing of bR and contacts along the *c* axis. The (*a*,*b*) plane, which is perpendicular to the *c* axis, corresponds to the plane of the membrane in the purple patches. The protein-protein interactions are limited in extent and involve mainly loops AB and BC (enlarged in insert I). A space-filling model of region II is shown in the corresponding insert. Color code for atoms: yellow, carbon; red, oxygen; blue, nitrogen; and green, sulfur.

been extended to 2.0 Å. Here, we present the 3D structure of this protein at a resolution of 2.5 Å, based on the analysis of data obtained with highly intense synchrotron radiation.

Preparation of monomeric bR and its crystallization from monoglyceride-based cubic phases were done as described (*12*, *13*). Thin hexagonal plates with dimensions of 20 to 40 μm by 20 to 40 μm by 5 μm formed readily and reproducibly within days from a monoolein-water cubic phase, yielding hundreds of crystals in each charge. The thinnest crystals consisted of about 500 unit cell layers along the *c* axis and exhibited the least mosaicity (a few tenths as compared with several degrees for larger crystals). The very intense microfocus beamline ID13 at the European Synchrotron Radiation Facility (ESRF) was required for data collection at high resolution. The best crystals (10% of all crystals examined) diffracted to 2.0 Å. The data from flash-frozen (100 K) crystals were integrated to 2.4 Å (Table 1). The space group was determined to be $P6_3$, with a unit cell of $a = b = 61.76$ Å, $c = 104.16$ Å, $\alpha = \beta = 90°$ and $\gamma = 120°$, and one monomer per asymmetric unit. The packing is dense; 62% of the volume is accounted for by protein, whereas the remainder is estimated to be distributed about equally between water and lipids. The monoolein-based cubic phase itself undergoes a reversible cubic-to-lamellar phase transition upon cooling (*14*). This transition of the phase surrounding the immobilized bR crystals does not affect the crystal quality.

Our current x-ray model of bR comprises 82% of the 248 amino acid residues (residues 7 to 156 and 167 to 225), the retinal, and 144 positions of atoms that correspond to water or lipid molecules (see below). Residues 1 to 6, 157 to 166, and 226 to 248 appear disordered and could not be reconstructed. The crystal packing shows protein layers stacked along the *c* axis with molecules related by a twofold screw axis (Fig. 1). The interactions along this direction are rather limited. Distinct protein-protein interactions exist only between loops AB (defined as the loop connecting helices A and B) and BC of two symmetry-related molecules (inserts in Fig. 1). The crystal contacts thus appear rather weak, consistent with

Table 1. Crystallization, data collection, and processing. Preparation of monomeric bR and its crystallization from monoolein-water cubic phases were as described (*12*, *13*). Data were collected at ESRF using the D2AM beamline for the characterization of crystals and space group determination. A data set to 4 Å resolution was collected on a single crystal over a range of 140° of rotation. High-resolution data on crystals cooled to 100 K were collected on beamline ID13 ($\lambda = 0.69$ Å) using a MARResearch imaging plate. The monoolein lipids composing the cubic phase provided cryoprotection. Data were integrated with the program DENZO (*30*) to 2.4 Å and processed using the CCP4 suite of programs (*31*). Molecular replacement was done on the basis of coordinates deposited in the Brookhaven Protein Data Bank that were determined by EM (*6*). The initial model, defined as a polyalanine and restricted to the helices, gave a valid starting model ($R_{free} = 43.4\%$, $R = 44.9\%$ from 8 to 4 Å). Side chains were progressively reconstructed from electron density maps ($2F_{obs} - F_{calc}$) weighted with the sigma-A procedure, using the program O (*32*). The structure was refined with X-PLOR, versions 3.1 and 3.8 (*33*), starting with rigid body refinements (8 to 3.5 Å) that were followed by energy minimization cycles, as well as simulated annealing and grouped temperature factor refinements between 6 and 2.8 Å. The resolution was progressively increased to 2.5 Å, and individual *B* factors were refined. An overall anisotropic *B* factor refinement showed no noticeable anisotropy along the *c* axis and did not improve the model. The refinement was done in different resolution shells ranging from 10 to 2.4 Å with or without bulk solvent corrections. The resolution shell from 5 to 2.5 Å was the most satisfactory because intensities from 2.5 to 2.4 Å are weak, and because partially ordered lipid molecules around the protein trimers might contribute strongly to the diffraction between 5 and 10 Å. Stereochemical values are all within the expected ranges for a 2.5 Å structure. All residues are in allowed regions of the Ramachandran plot. Coordinates and structure factors have been deposited in the Brookhaven Protein Data Bank (entry code 1AP9).

Resolution (Å)	10 to 2.4
$R_{sym}(I)$* (%)	10
Completeness (%)	91
Multiplicity	2
Refinement (5 to 2.5 Å)	
No. of unique reflections ($F > 3\sigma$)	5893
R_{free}† (%)	32.7
R factor‡ (%)	22.1
Non-hydrogen atoms	1761
Protein	1597
Cofactor	20
Water§	144
rms deviation on bond length (Å)	0.016
rms deviation on bond angles (°)	2.29
Average *B* factors (Å^2)	
Protein	54.1
Cofactor	54.6
Water§	57.0

*$R_{sym}(I) = \Sigma_{hkl}\Sigma_i|I_{hkl,i} - \langle I_{hkl}\rangle|/\Sigma_{hkl}\Sigma_i|I_{hkl,i}|$, where $\langle I_{hkl}\rangle$ is the average intensity of the multiple $I_{hkl,i}$ observations for symmetry-related reflections. †$R_{free} = \Sigma_{hkl\ \varepsilon\ T}|F_{obs} - F_{calc}|/\Sigma_{hkl\ \varepsilon\ T}|F_{obs}|$, where the T set (5% of the data) is omitted in the refinement. ‡*R* factor $= \Sigma_{hkl}|F_{obs} - F_{calc}|/\Sigma_{hkl}|F_{obs}|$. §Only water molecules with a temperature factor lower than 110 Å^2 were considered in the model building.

the observation that about 9 crystals out of 10 exhibit a large mosaicity along this axis. The packing of bR in the (*a*,*b*) plane (Fig. 2) is similar to that observed in the purple patches: The molecules are arranged in trimers with comparable unit cell dimensions. Loops CD, DE, and FG are well defined in the electron density maps ($2F_{obs} - F_{calc}$) and are also reflected by the refined temperature factors. Loops AB and BC are less well defined, and loop EF is not detected. Loops AB and CD account for the intratrimer contacts. No intertrimer protein contacts can be seen in the (*a*,*b*) plane (Fig. 2). Comparison between the x-ray and EM models (Fig. 3) reveals a high degree of similarity in the helical regions, as shown from the root-mean-square (rms) deviations (*15*). Markedly different conformations in loops AB and BC are observed (Fig. 3). Whether these differences are induced by the formation of crystal contacts is unknown.

The retinal, located deep within the protein (Fig. 4C), is the heart of bR. It is positioned between the two nearly parallel residues Trp^{86} and Trp^{182}, in agreement with the EM model. In both structures, the polyene chain is in the all-trans configuration. The extended polyene chain is found to be both slightly distorted and twisted out of plane (*16*), in agreement with an earlier simulation (*17*). The main residues participating in the proton translocation machinery—the Lys^{216} Schiff base, Asp^{85}, and Asp^{96}, identified unequivocally by site-specific mutagenesis—are well defined in our electron density maps. Arg^{82}, previously thought to form a salt bridge with Asp^{85} (*18*), is defined by a clear density in our map, with a distance to Asp^{85} incompatible with a salt bridge (Fig. 4D). We found excellent electron density around Glu^{204}, where our map shows the side chain pointing away from the proton channel; this finding is at variance with the EM model (Fig. 4E). This residue, located at the onset of helix G, is close to the extracellular side and has been suggested as a possible proton releasing group [(*18*, *19*), but see below]. The orientation of the side chain of Tyr^{57} is different as well, as is the hydrogen bond network around Asp^{212}, which in turn is hydrogen-bonded to Tyr^{57} and Tyr^{185}. A hydrogen bond to Trp^{86} is not observed (Fig. 4F).

For protons to overcome the distances between the amino acid residues involved in proton translocation, water molecules in the interior of bR appear to be inevitable constituents (*20*). We searched the electron density map for the presence of water molecules and identified 144 possible positions, of which 93 have a temperature factor (*B* value) smaller than 60 $Å^2$. Among them, at least eight water molecules are located in the putative proton channel between helices B, C, and G. Four of these could be identified unequivocally (Fig. 4A); of the remaining 136, some are located within bR

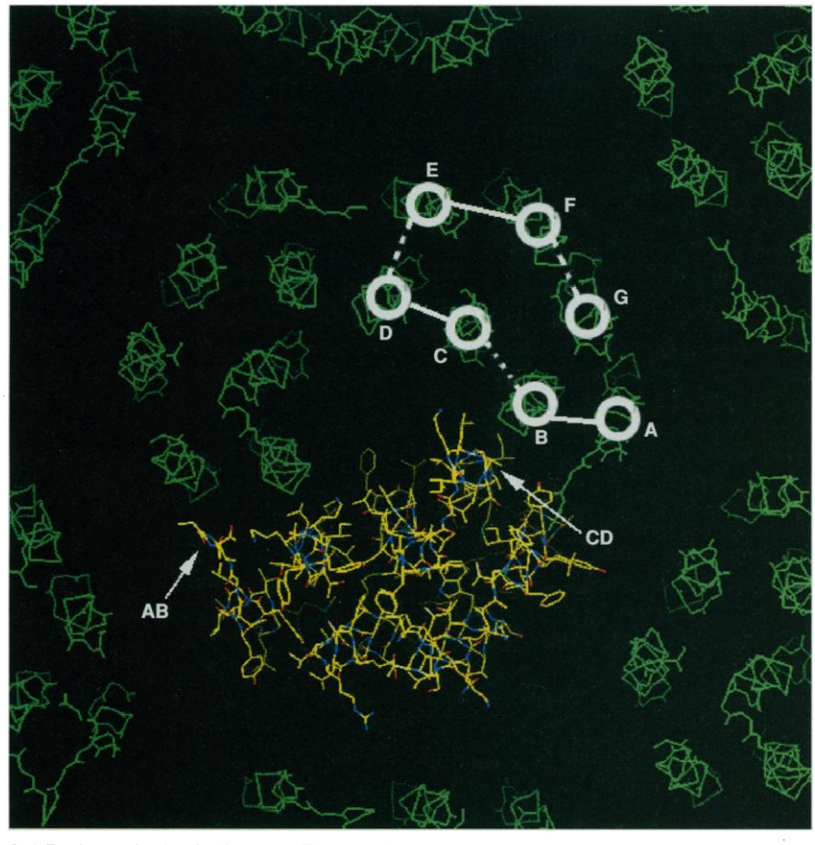

Fig. 2. bR trimers in the (*a*,*b*) plane. The view is along the *c* axis from the cytoplasmic toward the extracellular space. The schematic upper right sector defines the positions of the helices and connecting loops, drawn as solid lines on the cytoplasmic side and as dashed lines on the extracellular side. The upper left sector depicts the backbone of the helices in green. Loops AB and CD, which participate extensively in the intratrimer interactions, are highlighted in the lower sector, which reveals the backbone and side chain residues in stick models (color code as defined in Fig. 1).

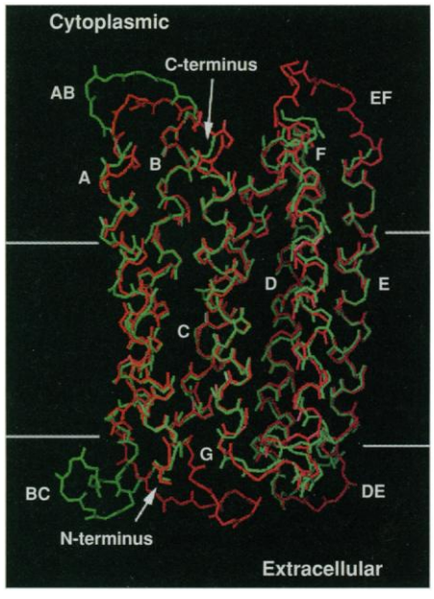

Fig. 3. View of the α helices of a bR monomer perpendicular to the membrane plane. The model derived from x-ray analysis is shown in green; the earlier model from EM (*6*) is represented in red. The retinal is not shown. The overall structure of bR is composed of seven helices [values in parentheses are from the EM model (*6*)]: A, residues 10 to 30 (9 to 31); B residues 39 to 62 (39 to 62); C, residues 77 to 101 (77 to 100); D, residues 105 to 127 (105 to 127); E, residues 134 to 156 (134 to 157); F, residues 169 to 191 (166 to 190); and G, residues 202 to 224 (202 to 226). The backbones superimpose very well in the helical transmembrane regions, but distinct differences are revealed in loops AB (upper left) and BC (lower left). N-terminal residues 1 to 6 and C-terminal residues 225 to 248, as well as loop EF (residues 157 to 166, upper right), are absent in the x-ray structure and the EM model. Helices C and G deviate from standard α-helical geometry at residues 89 and 216, respectively. In the EM model, deviations (kinks) are observed in helices B, C, and F for residues 46 to 49, 87 to 90, and 182 to 185, respectively, but not in helix G. The horizontal lines delimit the hydrophobic core of bR.

boundaries but not in the putative proton channel, and thus they may represent structural water molecules. The other water molecules are distributed among two populations. The first is located on the surface of the trimer and is exposed to bulk solvent, which at this stage of the refinement may either be ordered water or missing loops. The second is located laterally around the trimers and may correspond to lipids, but an unequivocal identification requires further investigation. Higher resolution and better quality data should allow water to be distinguished from lipid molecules in that location.

Within the channel, the photoexcited protonated Schiff base releases its proton to Asp[85] toward the extracellular side. Its car-

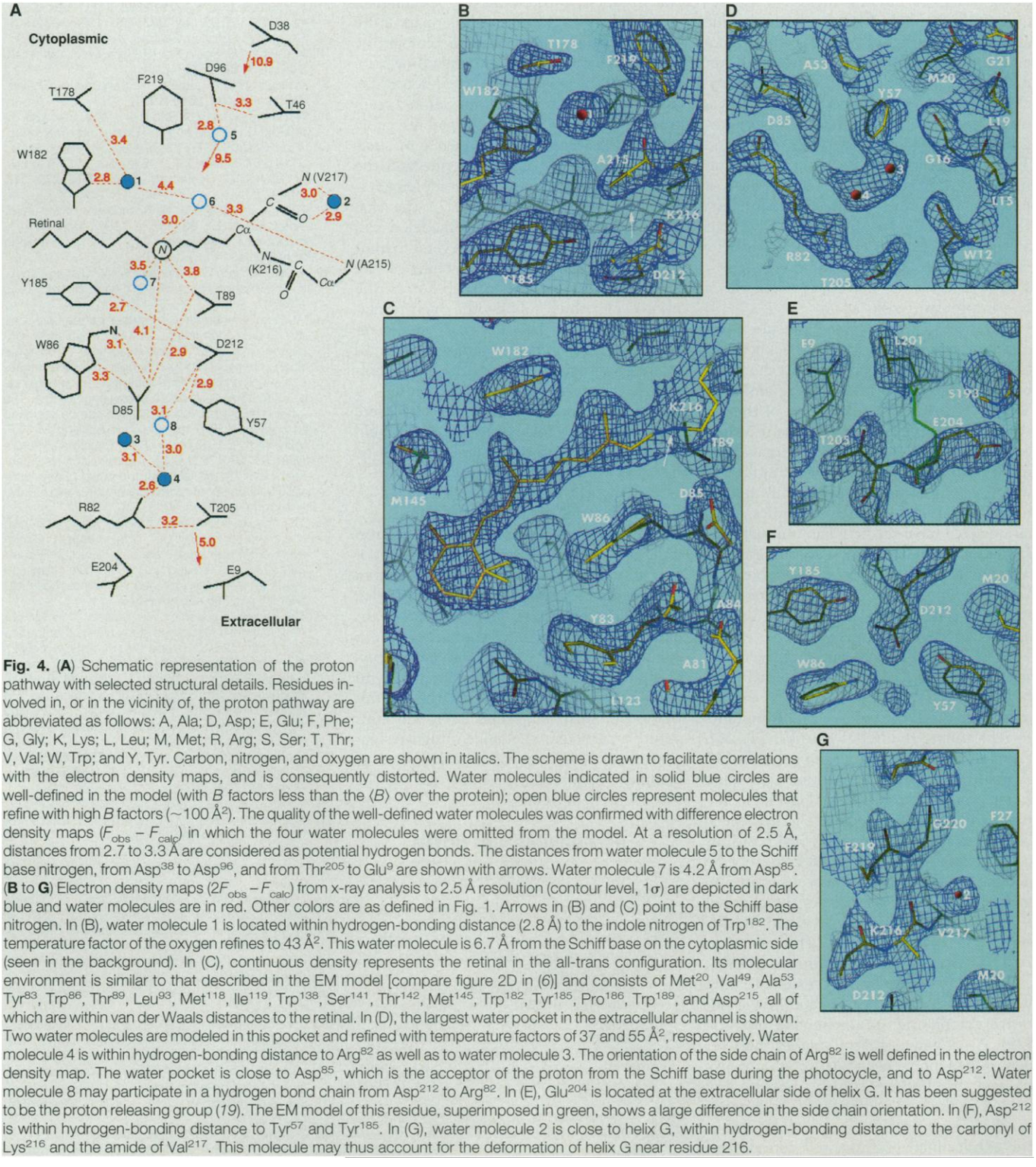

Fig. 4. (**A**) Schematic representation of the proton pathway with selected structural details. Residues involved in, or in the vicinity of, the proton pathway are abbreviated as follows: A, Ala; D, Asp; E, Glu; F, Phe; G, Gly; K, Lys; L, Leu; M, Met; R, Arg; S, Ser; T, Thr; V, Val; W, Trp; and Y, Tyr. Carbon, nitrogen, and oxygen are shown in italics. The scheme is drawn to facilitate correlations with the electron density maps, and is consequently distorted. Water molecules indicated in solid blue circles are well-defined in the model (with *B* factors less than the ⟨*B*⟩ over the protein); open blue circles represent molecules that refine with high *B* factors (~100 Å^2). The quality of the well-defined water molecules was confirmed with difference electron density maps ($F_{obs} - F_{calc}$) in which the four water molecules were omitted from the model. At a resolution of 2.5 Å, distances from 2.7 to 3.3 Å are considered as potential hydrogen bonds. The distances from water molecule 5 to the Schiff base nitrogen, from Asp[38] to Asp[96], and from Thr[205] to Glu[9] are shown with arrows. Water molecule 7 is 4.2 Å from Asp[85]. (**B** to **G**) Electron density maps ($2F_{obs} - F_{calc}$) from x-ray analysis to 2.5 Å resolution (contour level, 1σ) are depicted in dark blue and water molecules are in red. Other colors are as defined in Fig. 1. Arrows in (B) and (C) point to the Schiff base nitrogen. In (B), water molecule 1 is located within hydrogen-bonding distance (2.8 Å) to the indole nitrogen of Trp[182]. The temperature factor of the oxygen refines to 43 Å^2. This water molecule is 6.7 Å from the Schiff base on the cytoplasmic side (seen in the background). In (C), continuous density represents the retinal in the all-trans configuration. Its molecular environment is similar to that described in the EM model [compare figure 2D in (*6*)] and consists of Met[20], Val[49], Ala[53], Tyr[83], Trp[86], Thr[89], Leu[93], Met[118], Ile[119], Trp[138], Ser[141], Thr[142], Met[145], Trp[182], Tyr[185], Pro[186], Trp[189], and Asp[215], all of which are within van der Waals distances to the retinal. In (D), the largest water pocket in the extracellular channel is shown. Two water molecules are modeled in this pocket and refined with temperature factors of 37 and 55 Å^2, respectively. Water molecule 4 is within hydrogen-bonding distance to Arg[82] as well as to water molecule 3. The orientation of the side chain of Arg[82] is well defined in the electron density map. The water pocket is close to Asp[85], which is the acceptor of the proton from the Schiff base during the photocycle, and to Asp[212]. Water molecule 8 may participate in a hydrogen bond chain from Asp[212] to Arg[82]. In (E), Glu[204] is located at the extracellular side of helix G. It has been suggested to be the proton releasing group (*19*). The EM model of this residue, superimposed in green, shows a large difference in the side chain orientation. In (F), Asp[212] is within hydrogen-bonding distance to Tyr[57] and Tyr[185]. In (G), water molecule 2 is close to helix G, within hydrogen-bonding distance to the carbonyl of Lys[216] and the amide of Val[217]. This molecule may thus account for the deformation of helix G near residue 216.

boxyl group remains protonated until the last step of the photocycle (*21*). Asp^{85} resides within hydrogen-bonding distance of both Trp^{86} and Thr^{89}. We did not find any water molecules within hydrogen-bonding distance of Asp^{85}. Retinal isomerization seems to cause rearrangement of the neighboring residues, in particular Trp^{86}, thereby destabilizing its binding to Asp^{85}. Consequently, it is likely that the latter residue approaches the Schiff base, allowing direct proton transfer to occur. The water pocket near Asp^{85}, Tyr^{57}, Asp^{212}, and Arg^{82}, including water molecules 3 and 4, forms a hydrogen bond network that facilitates proton translocation from Asp^{85} to Arg^{82} and Thr^{205} (Fig. 4D). Such a delocalized proton transfer was indeed observed on the basis of Fourier transform infrared experiments (*22*). Because Glu^{9} is situated near the exit of the proton channel (Fig. 4E), with its carboxylate group 5 Å from Thr^{205}, a possible rotation of the side chain might play a role in proton translocation.

The well-defined water molecule 2, located in the vicinity of the backbone of helix G, forms hydrogen bonds to the backbone carbonyl of Lys^{216} and the amide of Val^{217} (Fig. 4G). The deviation of the geometry of helix G from standard values between residues 216 and 217 may be a result of the binding of this water molecule, which would compete with an intrahelical hydrogen bond. Molecular dynamics simulations (*10*) have predicted an unusual conformation of helix G and the binding of a water molecule to the backbone carbonyl of Lys^{216}. A water network in an intermediate state (M state) has been suggested on the basis of spectroscopic analyses (*23*).

In the cytoplasmic segment of the channel, water molecule 1 forms a hydrogen bond to Trp^{182} (Fig. 4B). Asp^{96} is known from time-resolved studies with bR mutants to reprotonate the Schiff base (*9*, *21*, *24*). From our structure, this residue is located 10 Å from the Schiff base, a distance too large for a proton transfer step (Fig. 4A). We found that water molecule 5 is hydrogen-bonded to Asp^{96}, but unequivocal positions of additional water molecules could not be detected in this region. The proton pathway in the cytoplasmic segment of the channel is therefore not uniquely defined at this time. The portion of the channel from Asp^{96} to the cytoplasmic surface is delimited by Asp^{38} and could be accessible to bulk water. Asp^{38} is the first residue in the putative cytoplasmic proton uptake pathway (*25*). A p*K* value of Asp^{96} higher than 11, determined previously (*26*), could be explained by limited solvent accessibility caused by the position of Phe^{42}. In summary, the positions of the water molecules in the extracellular part are well defined and support our proposed proton pathway, whereas the mechanism of translocation in the more hydrophobic cytoplasmic channel remains to be elucidated.

Our high-resolution 3D structure of bR identifies the locations of water molecules within this membrane protein. Thus, the structural basis for the mechanism of proton translocation, hitherto largely speculative, is set, at least in the extracellular part of the channel. The x-ray structure is biologically relevant, because bR in the crystalline state undergoes the main steps in the photocycle, as shown by Fourier transform infrared spectroscopy in the fully transparent cubic phase (*27*). Also, the high degree of similarity between the x-ray structure and the EM model demonstrates the complementarity of these methods: Most of the side chains that were previously modeled can now be established, whereas several exhibit distinct differences. Our structure of the ground state represents a snapshot in the photocycle; thus, solving the high-resolution structure of the M state(s) should reveal differences in the protein structure and altered positions of some of the water molecules. This should eventually provide a basis for the understanding of the complete photocycle at atomic resolution, and should allow the plethora of earlier studies to be interpreted in structural terms.

Solving the structure of bR to 2.5 Å from very small crystals affirms the potential of the latest generation of synchrotron radiation sources. Moreover, the concept of crystallization of membrane proteins from 3D membrane-mimetic matrices, afforded by lipidic cubic phases (*12*), is clearly validated and was critical for the success of our studies. Attempts to design the "mesh sizes" of such matrices (*12*, *13*, *28*), in analogy to crystal engineering devised for the crystallization of small molecules (*29*), will constitute a particular challenge if high-resolution x-ray structures of a wide range of complex membrane proteins are to be solved in the future.

REFERENCES AND NOTES

1. D. Oesterhelt, J. Tittor, E. Bamberg, *J. Bioenerg. Biomem.* **24**, 181 (1992).
2. D. Oesterhelt and W. Stoeckenius, *Proc. Natl. Acad. Sci. U.S.A.* **70**, 2853 (1973).
3. R. Henderson and P. N. T. Unwin, *Nature* **257**, 28 (1975); P. N. T. Unwin and R. Henderson, *J. Mol. Biol.* **94**, 425 (1975).
4. R. Henderson, *J. Mol. Biol.* **93**, 123 (1975); A. E. Blaurock, *ibid.*, p. 139.
5. R. Henderson *et al.*, *ibid.* **213**, 899 (1990).
6. N. Grigorieff, T. A. Ceska, K. H. Downing, J. M. Baldwin, R. Henderson, *ibid.* **259**, 393 (1996).
7. D. M. Engelman, R. Henderson, A. D. McLachlan, B. A. Wallace, *Proc. Natl. Acad. Sci. U.S.A.* **77**, 2023 (1980).
8. Y. A. Ovchinnikov, N. G. Abdulaev, M. Y. Feigina, A. V. Kiselev, N. A. Lobanov, *FEBS Lett.* **100**, 219 (1979); H. G. Khorana *et al.*, *Proc. Natl. Acad. Sci. U.S.A.* **76**, 5046 (1979); H. G. Khorana, *J. Biol. Chem.* **263**, 7439 (1988); N. A. Dencher, D. Dresselhaus, G. Zaccai, G. Büldt, *Proc. Natl. Acad. Sci. U.S.A.* **86**, 7876 (1989); B. F. Ni, M. Chang, A. Duschl, J. Lanyi, R. Needleman, *Gene* **90**, 169 (1990); M. P. Krebs, T. Hauss, M. P. Heyn, U. L. Rajbhandary, H. G. Khorana, *Proc. Natl. Acad. Sci. U.S.A.* **88**, 859 (1991); R. A. Mathies, S. W. Lin, J. B. Ames, W. T. Pollard, *Annu. Rev. Biophys. Chem.* **20**, 491 (1991); J. Sasaki, Y. Shichida, J. K. Lanyi, A. Maeda, *J. Biol. Chem.* **267**, 20782 (1992); J. K. Lanyi, *Biochim. Biophys. Acta* **1183**, 241 (1993); M. Ferrand *et al.*, *FEBS Lett.* **327**, 256 (1993); D. Xu, M. Sheves, K. Schulten, *Biophys. J.* **69**, 2745 (1995).
9. K. Gerwert, G. Souvignier, B. Hess, *Proc. Natl. Acad. Sci. U.S.A.* **87**, 9774 (1990).
10. W. Humphrey, I. Logunov, K. Schulten, M. Sheves, *Biochemistry* **33**, 3668 (1994).
11. R. Henderson and D. Shotton, *J. Mol. Biol.* **139**, 99 (1980); H. Michel and D. Oesterhelt, *Proc. Natl. Acad. Sci U.S.A.* **77**, 1283 (1980); H. Michel, *EMBO J.* **1**, 1267 (1982); G. F. X. Schertler, H. D. Bartunik, H. Michel, D. Oesterhelt, *J. Mol. Biol.* **234**, 156 (1993).
12. E. M. Landau and J. P. Rosenbusch, *Proc. Natl. Acad. Sci. U.S.A.* **93**, 14532 (1996). Monoolein (1-monooleoyl-*rac*-glycerol, $C_{18:1c9}$) was obtained from Sigma.
13. E. M. Landau, G. Rummel, S. W. Cowan-Jacob, J. P. Rosenbusch, *J. Phys. Chem. B* **101**, 1935 (1997).
14. At room temperature, a powder pattern with one strong diffraction ring at 53 Å (accessible low-resolution limit is 60 Å) was observed. Upon rapid cooling to liquid nitrogen temperature, the diffraction image changed to multiple low-resolution rings at 52 Å, 25 Å, 12 Å, and a strong ring at 4.5 Å. The latter is also observed at 4°C and can be assigned to the periodicity of the lipid chain packing [M. H. F. Wilkins, A. E. Blaurock, D. M. Engelman, *Nature New Biol.* **230**, 72 (1971)]. This transition also manifests itself by the fact that the cubic phase, optically transparent at room temperature, turns slightly opaque upon cooling.
15. The rms deviations are 0.7 and 1.2 Å for the main chain and for all the non-hydrogen atoms, respectively, if only the helices are considered. This compares with rms deviations of 3.6 Å (main chain) and 4.0 Å (all non-hydrogen atoms) if all residues between 7 and 225 are included.
16. The degree of distortion was unclear. A recent nuclear magnetic resonance study claims that the angles for the C18, C19, and C20 methyl groups with the membrane normal are 37°, 40°, and 32°, respectively [A. S. Ulrich, A. Watts, I. Wallat, M. P. Heyn, *Biochemistry* **33**, 5370 (1994)], whereas the EM structure represents them as 38.6°, 29.3°, and 16.1°, respectively. Our structure reveals values of 32°, 34°, and 10°, respectively.
17. K. Schulten and P. Tavan, *Nature* **272**, 85 (1978).
18. C. Scharnagl, J. Hettenkofer, S. F. Fischer, *J. Phys. Chem.* **99**, 7787 (1995).
19. L. S. Brown *et al.*, *J. Biol. Chem.* **270**, 27122 (1995).
20. G. Papadopoulos, N. A. Dencher, G. Zaccai, G. Büldt, *J. Mol. Biol.* **214**, 15 (1990).
21. M. S. Braiman *et al.*, *Biochemistry* **27**, 8516 (1988).
22. J. Le Coutre and K. Gerwert, *FEBS Lett.* **398**, 333 (1996).
23. H. Takei, Y. Gat, Z. Rothman, A. Lewis, M. Sheves, *J. Biol. Chem.* **269**, 7387 (1994).
24. J. Tittor, U. Schweiger, D. Oesterhelt, E. Bamberg, *Biophys. J.* **67**, 1682 (1994).
25. J. Riesle, D. Oesterhelt, N. A. Dencher, J. Heberle, *Biochemistry* **35**, 6635 (1996).
26. S. Szaraz, D. Oesterhelt, P. Ormos, *Biophys. J.* **67**, 1706 (1994).
27. J. Heberle and E. M. Landau, unpublished results.
28. G. Lindblom and L. Rilfors, *Biochim. Biophys. Acta* **988**, 221 (1989).
29. I. Weissbuch, R. Popovitz-Biro, M. Lahav, L. Leiserowitz, *Acta Crystallogr.* **B51**, 115 (1995); V. A. Russell, C. C. Evans, W. Li, M. D. Ward, *Science* **276**, 575 (1997).
30. Z. Otwinowski, in *Data Collection and Processing*, L. Sawyer, N. Isaacs, S. Bailey, Eds. (SERC Daresbury

Laboratory, Warrington, UK, 1993), pp. 56–62.
31. Collaborative Computation Project 4, *Acta Crystallogr.* **D50**, 760 (1994).
32. A. T. Jones, J. Y. Zou, S. W. Cowan, M. Kjeldgaard, *ibid.* **A47**, 110 (1991).
33. A. T. Brünger, *X-PLOR, Version 3.1: A System for X-ray Crystallography and NMR* (Yale Univ. Press, New Haven, CT, 1992).
34. We thank C. Riekel, H. Belrahli, and A. Bram for invaluable help on the ID13 beamline; E. Fanchon, R. Kahn, and M. Roth on the French beamline D2AM; G. Büldt for his generosity; G. Büldt, S. Cusack, O. Dideberg, J. Heberle, J. Sass, and G. Zaccai for stimulating discussions; and T. Bickle and R. Eisenberg for critically reading the manuscript. Supported by the Université Joseph Fourier, the Institut de Biologie Structurale, the Institut Universitaire de France, the University of Basel, and grants from the Swiss National Science Foundation (SPP 5002-37911 and -46092), EU-BIOMED (BIO4CT96/BBW95.0137.2), and EU-BIOTECH (EU-BIO4CT96/BBW96.0145.1). Beam time at the ESRF (Grenoble, France) was granted under experiments LS-435, LS-553, LS-655, 02.03.060, and 02.03.111.

11 June 1997; accepted 28 July 1997

Cysteine and Glutathione Secretion in Response to Protein Disulfide Bond Formation in the ER

Stephana Carelli, Aldo Ceriotti, Andrea Cabibbo, Giorgio Fassina, Menotti Ruvo, Roberto Sitia*

Protein folding in the endoplasmic reticulum (ER) often involves the formation of disulfide bonds. The oxidizing conditions required within this organelle were shown to be maintained through the release of small thiols, mainly cysteine and glutathione. Thiol secretion was stimulated when proteins rich in disulfide bonds were translocated into the ER, and secretion was prevented by the inhibition of protein synthesis. Endogenously generated cysteine and glutathione counteracted thiol-mediated retention in the ER and altered the extracellular redox. The secretion of thiols might link disulfide bond formation in the ER to intra- and intercellular redox signaling.

The ER is the port of entry and main folding compartment for proteins destined for the central vacuolar system (*1*). Nascent proteins are translocated into the ER in the reduced state and rapidly form disulfides in the suitable redox environment of this organelle (*2*, *3*). Oxidizing conditions are likely to be generated by the import of oxidized glutathione (GSSG) and cystine (*3*) and must be continuously maintained to counteract the vectorial import of reduced cysteine residues that enter the ER as part of the translocated polypeptides. Imported GSSG and cystine can participate in disulfide interchange reactions involving ER-resident as well as newly made proteins (*3*, *4*) and catalyzed by protein disulfide isomerase, ERp72, and other oxidoreductases (*1*, *2*). It is possible that the homeostasis of the redox state in the ER depends on the flux of small disulfides, secreted together with their reduced counterparts, which are generated during the process of protein disulfide bond formation.

To test this model, we monitored the accumulation of thiols in the extracellular space (Fig. 1). As observed for other cell types (*3*), both J558L myeloma cells (Fig. 1, A and C) and *Xenopus laevis* oocytes (Fig. 1E) released thiols. The export of thiols and of constitutively secreted proteins [immunoglobulin (Ig) λ chains] was compared in J558L cells after perturbation of vesicular traffic by treatment at low temperature (20°C) or in the presence of brefeldin A (BFA) (*5*). After the first hour of treatment, the extracellular accumulation of both λ chains and thiols was inhibited (Fig. 1), which suggested that a functional secretory apparatus was required for their release. When cells were kept at 20°C for 3 hours and then transferred to 37°C, the secretion of both thiols and proteins was promptly restored (Fig. 1, A and B). The similar behavior of thiols and λ chains suggests that they did indeed utilize the same transport systems. In agreement with previous observations that J558L cells secrete λ chains that are completely oxidized (*4*), virtually all secreted thiols were soluble in acetone (*6*). Differences in the equilibrium constant (K_{ox}) may explain the coexistence of reduced glutathione and cysteine with oxidized proteins (*7*). Similar findings were also obtained with isolated amphibian oocytes, in which monensin, another inhibitor of protein secretion, inhibited thiol release (Fig. 1E). Monensin was used because BFA is ineffective in *Xenopus* oocytes (*8*).

We also predicted that thiol release should be influenced by the synthesis of secretory proteins containing disulfide bonds. In agreement with this, cyclohexi-

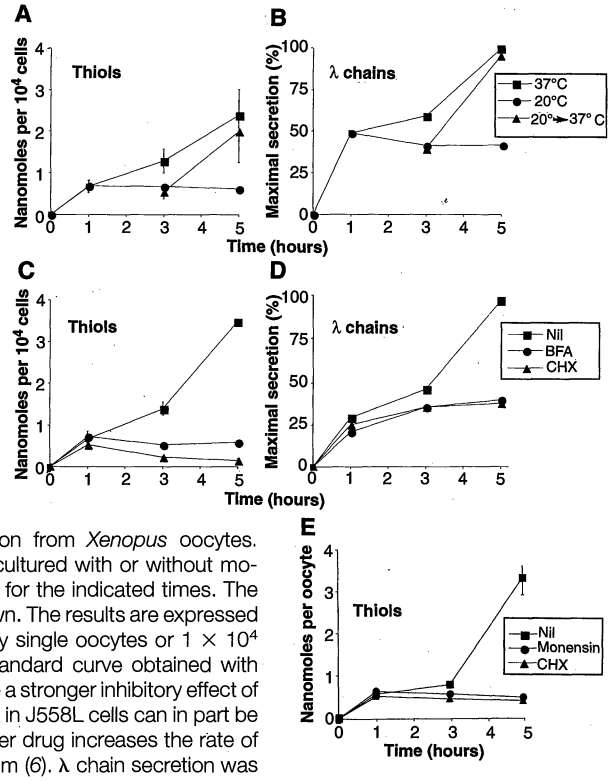

Fig. 1. Thiol release through the secretory pathway requires protein synthesis. (**A** through **D**) J558L cells were cultured in a water bath for the indicated times at 20° or 37°C. After 3 hours, aliquots of cells cultured at 20°C were further cultured for 2 hours at 37°C [(A) and (B)]. J558L cells were cultured in an incubator at 37°C with or without BFA (5 μg/ml) or 500 μM cycloheximide (CHX) [(C) and (D)]. The spent media were harvested by centrifugation and the accumulation of thiols [(A) and (C), mean of three experiments], and λ chains [(B) and (D)] were quantitated by the 5,5′-dithiobis(2-nitrobenzoic acid) (DTNB) assay (*20*) and immunoblotting (*4*), respectively. (**E**) Thiol secretion from *Xenopus* oocytes. Groups of five oocytes (*21*) were cultured with or without monensin (20 μg/ml) or 500 μM CHX for the indicated times. The average of two experiments is shown. The results are expressed as nanomoles of thiols secreted by single oocytes or 1×10^4 J558L cells, as derived from a standard curve obtained with purified cysteine. What seems to be a stronger inhibitory effect of CHX as compared with that of BFA in J558L cells can in part be explained by the fact that the former drug increases the rate of decay of thiols in the culture medium (*6*). λ chain secretion was normalized assuming as 100% the amount of protein present in control cultures at 5 hours.

S. Carelli, A. Cabibbo, R. Sitia, DIBIT, Istituto Scientifico San Raffaele, Milano, Italy.
A. Ceriotti, Istituto Biosintesi Vegetali, Consiglio Nazionale delle Ricerche, Milano, Italy.
G. Fassina and M. Ruvo, Tecnogen, Piana di Monte Verna (CE), Italy.
*To whom correspondence should be addressed. E-mail: sitiar@dibit.hsr.it